Mon. Not. R. Astron. Soc. **000**, 1–16 (2016) Printed 18 August 2016 (MN LATEX style file v2.2)

The *Chandra* ACIS Timing Survey Project: glimpsing a sample of faint X-ray pulsators

G. L. Israel,[1⋆] P. Esposito,[2,3] G. A. Rodríguez Castillo[1] and L. Sidoli[3]

[1]*INAF–Osservatorio Astronomico di Roma, via Frascati 33, I-00040 Monteporzio Catone, Italy*
[2] *Anton Pannekoek Institute for Astronomy, University of Amsterdam, Postbus 94249, NL-1090-GE Amsterdam, The Netherlands*
[3]*INAF–Istituto di Astrofisica Spaziale e Fisica Cosmica - Milano, via E. Bassini 15, I-20133 Milano, Italy*

arXiv:1608.00077v2 [astro-ph.HE] 17 Aug 2016

Accepted 2016 July 27. Received 2016 July 23; in original form 2016 April 13

ABSTRACT

We report on the discovery of 41 new pulsating sources in the data of the *Chandra* Advanced CCD Imaging Spectrometer, which is sensitive to X-ray photons in the 0.3–10 keV band. The archival data of the first 15 years of *Chandra* observations were retrieved and analysed by means of fast Fourier transforms, employing a peak-detection algorithm able to screen candidate signals in an automatic fashion. We carried out the search for new X-ray pulsators in light curves with more than 50 photons, for a total of about 190 000 lightcurves out of about 430 000 extracted. With these numbers, the ChAndra Timing Survey at Brera And Roma astronomical observatories (CATS @ BAR)—as we called the project—represents the largest ever systematic search for coherent signals in the classic X-ray band. More than 50 per cent of the signals were confirmed by further *Chandra* (for those sources with two or more pointings), *XMM–Newton* or *ROSAT* data. The period distribution of the new X-ray pulsators above $\sim$2 000 s resembles that of cataclysmic variables, while there is a paucity of sources with shorter period and low fluxes. Since there is not an obvious bias against these detections, a possible interpretation is in terms of a magnetic gating mechanism in accreting neutron stars. Finally, we note that CATS @ BAR is a living project and the detection algorithm will continue to be routinely applied to the new *Chandra* data as they become public. Based on the results obtained so far, we expect to discover about three new pulsators every year.

Key words: catalogues – methods: data analysis – pulsars: general – stars: oscillations – X-rays: binaries – X-rays: stars

1 INTRODUCTION

The detection and characterization of X-ray periodic signals play a role of paramount importance in the process of identifying new compact objects or new classes of them, and studying the mechanisms powering the observed emission. Even new emission mechanisms have been discovered in this way. The greatest part of the periodic signals arise from the rotation of a compact star or from the orbital motion in a binary system. The main cases in which the modulation is due to the compact star spin are: (a) accreting magnetic neutron stars (NSs) in X-ray binary systems; (b) spinning down isolated NSs, the emission of which may be powered by the dissipation of rotational, thermal, or even magnetic energy (as in the cases of classical radio pulsars, X-ray dim isolated NSs, and magnetars, respectively); (c) magnetic white dwarf (WD) systems, such as polars and intermediate polars (IPs). Orbital modulations of the X-ray flux are observed in many classes of NS and black hole (BH) X-ray binaries and cataclysmic variables (CVs).

The discovery of a periodic modulation generally happens through the timing analysis of the X-ray light curves of the sources which lie in the field of view, FoV, of a detector. However, for most observations taken with imaging instruments, only the target of the pointing is analysed. With the high energy missions currently operational (such as *Chandra* or *XMM–Newton*), which have wide energy ranges, high sensitivities and, often, high time resolution, the average number of serendipitous X-ray sources detected is of the order of few tens. In a typical *Chandra* observation this number is $\sim$40[1]. During observations targeting crowded fields and in which all the CCDs were operating (each CCD covers 8.3′x 8.3′), up to about 100 sources can be detected. It is therefore evident that up to 99% of the information remain unexplored. Since the number of high quality time series stored in the present-day X-ray archives has now reached $\sim 10^6$, these data clearly hold a huge potential for new discoveries and make data mining an urgent task to achieve them.

Various projects aimed at the search for X-ray pulsators were

⋆ E-mail: gianluca@oa-roma.inaf.it

[1] This number is simply the ratio between detected sources, 430 000, and analysed datasets, 10 700; see also end of this Section.

© 2016 RAS

carried out in the past. During the 1990s, our team carried out systematic timing analyses of the then-booming number of bright serendipitous sources—about 50 000 objects detected with *ROSAT* and *EXOSAT* (Israel et al. 1998). The effort was based on discrete fast Fourier transform (FFT) analysis and resulted, among other findings, in the detection of pulsations from sources which have become prototypes of new classes, such as the anomalous X-ray pulsars (4U 0142+614; Israel et al. 1994) and the double-degenerate ultra-short period X-ray binaries hosting two WDs (HM Cnc; Israel et al. 2002). Remarkably, these sources are supposed to be powered by new and unusual mechanisms, such as the decay of the intense magnetic field (see Turolla et al. 2015 for a recent review) in the case of magnetars, and owing to the unipolar inductor model for ultra-compact binaries (Dall'Osso et al. 2006). We also discovered an X-ray pulsator in a binary systems in a previously unobserved evolutionary phase, a post-common envelope stage: HD 497985 (RX J0648.0–4418). It is a 13-s-period source which hosts either one of the most massive and fastest spinning WDs observed so far, or an unusual accreting NS spinning up at a low and extremely steady rate (Israel et al. 1997; Mereghetti et al. 2009, 2016).

More recently, several searches were conducted by other teams on *Chandra* and *XMM–Newton* data for a relatively limited number of objects or sky regions. Muno et al. (2003) searched for periodic signals among 285 sources detected with *Chandra* in the Galactic center region (about 500 ks of exposure time) by means of a Z_1^2 (Rayleigh) test (Buccheri et al. 1983). They found eight sources showing pulsations, with periods from $\sim$300 to 17 000 s. Muno et al. (2008) analysed almost 1 000 *Chandra* and *XMM–Newton* archival observations of the Galactic plane region ($|b| < 5^\circ$). All the detected sources were searched for coherent signals with a Rayleigh test for the *Chandra* data and a discrete FFTs for *XMM–Newton* data. Four sources with periodic modulations in the 200–5 000 s range were discovered and tentatively classified as CVs. Laycock et al. (2010) analysed two *Chandra* deep fields in the Small Magellanic Cloud (SMC), where almost 400 sources were detected and searched for pulsations. Two new accreting pulsars in high mass X-ray binaries (HMXBs) were discovered using the Lomb–Scargle method (LS; Scargle 1982). Hong et al. (2012) searched about 400 sources in 1-Ms *Chandra* data of the 'Limiting Window' region. A LS analysis led to the discovery of ten new X-ray sources with periods between 4 700 and 12 100 s; in three cases the signal was detected with good confidence (>99%). In a sample of 4 330 sources of the Second *XMM–Newton* Serendipitous Source Catalogue (2XMMi-DR3; Watson et al. 2009) which were reliably detected and observed at least twice, Lin, Webb, & Barret (2014) identified about 200 compact object candidates. By a FFT analysis, they found two sources which also show significant coherent pulsations (in the 5 000–8 000 s range). A Random Forest machine learning algorithm was employed by Farrell et al. (2015) to classify 2 876 variable *XMM–Newton* sources in the Third *XMM–Newton* Serendipitous Source Catalogue (3XMMi-DR4; Rosen et al. 2016). Two out of the about 100 unclassified objects showed in LS periodograms significant modulations at 400 and 18 000 s, identified with a spin and an orbital period, respectively. Finally, it is worth mentioning the results obtained by *Fermi* in the systematic 'blind' search for γ-ray pulsars, although in a different energy band (about 100 MeV–100 GeV), by means of FFT analysis carried out on photon time differences instead of event times (Atwood et al. 2006). This method made it possible to discover more than 50 new γ-ray pulsars[2] (Abdo et al. 2009).

In this paper, we report on the results of our search for new X-ray pulsators in all the archival data of the *Chandra* Advanced CCD Imaging Spectrometer (ACIS; Garmire et al. 2003) Imaging (I) or Spectroscopic (S) array in imaging mode. We analysed about 10 700 datasets, corresponding to the first $\sim$15 years of *Chandra* operations, and applied a FFT analysis coupled with an *ad hoc* signal detection algorithm to about 190 000 of about 430 000 light curves extracted (those with enough photons, >50, to allow a meaningful search). The ChAndra Timing Survey at Brera And Roma astronomical observatories (CATS @ BAR), as we called the project, is the largest ever systematic search for coherent signals in the classic X-ray band. Among the aims of CATS @ BAR there are: (i) to identify intrinsically faint X-ray pulsators at a flux level which has remained unexplored so far; (ii) to extend the validity of already known emission mechanisms towards lower X-ray fluxes; (iii) to look for new classes of compact objects and new astrophysical objects showing coherent signals. We found 41 new X-ray pulsators, with periods in the 8–64 000 s range. For a relatively large fraction of them, we rely upon more than one archival pointing allowing us to check for the reliability of the signal detection. A by-product of our systematic search analysis is a detailed map of the spurious (instrumental) coherent signals which affect the ACIS.

2 METHODOLOGY

Fourier analysis is likely the single most important technique which is applied to astronomical time series to detect signals through the presence of peaks in the power spectra and characterise the noise variability through the study of continuum power spectrum components (see Graham et al. 2013 for a comparison among different signal search algorithms). A periodic signal is identified when the strength of the corresponding peak is so high to make it stand out in the power spectral density (PSD), and is validated (at a given confidence level) against the chance that the peak originates from the underlying white noise. This approach assumes that the power spectra are dominated by Poissonian counting statistics. However, this is often not the case, at least over a range of frequencies (see left panel of Figure 1). Indeed, the presence of continuum non-Poissonian components in the power spectrum, resulting from intrinsic or instrumental variability in the source and/or the background, makes the detection of genuinely astrophysical signals a difficult statistical problem. Additionally, the number of serendipitous sources for which the timing analysis can be performed has became so large that it is virtually impossible to rely upon an inspection by eye of all the PSD produced in a large search to investigate every candidate signal.

An algorithm to search for coherent signals in a large number of sources needs to include a reliable automatic procedure to perform a first screening of possible signals. In our timing analysis we used the original (unbinned) event list extracted for each source in order to avoid, among others, issues due to the starting time of the series (middle time of the bin versus start of the time bin), a problem often met in the astronomical timing software when binned light curves are used. For the power spectrum density analysis we adopted the recipe outlined in Israel & Stella (1996),

[2] For an updated list, see https://confluence.slac.stanford.edu/display/GLAMCOG/Public+List+of+LAT-Detected+Gamma-Ray+Pulsars.

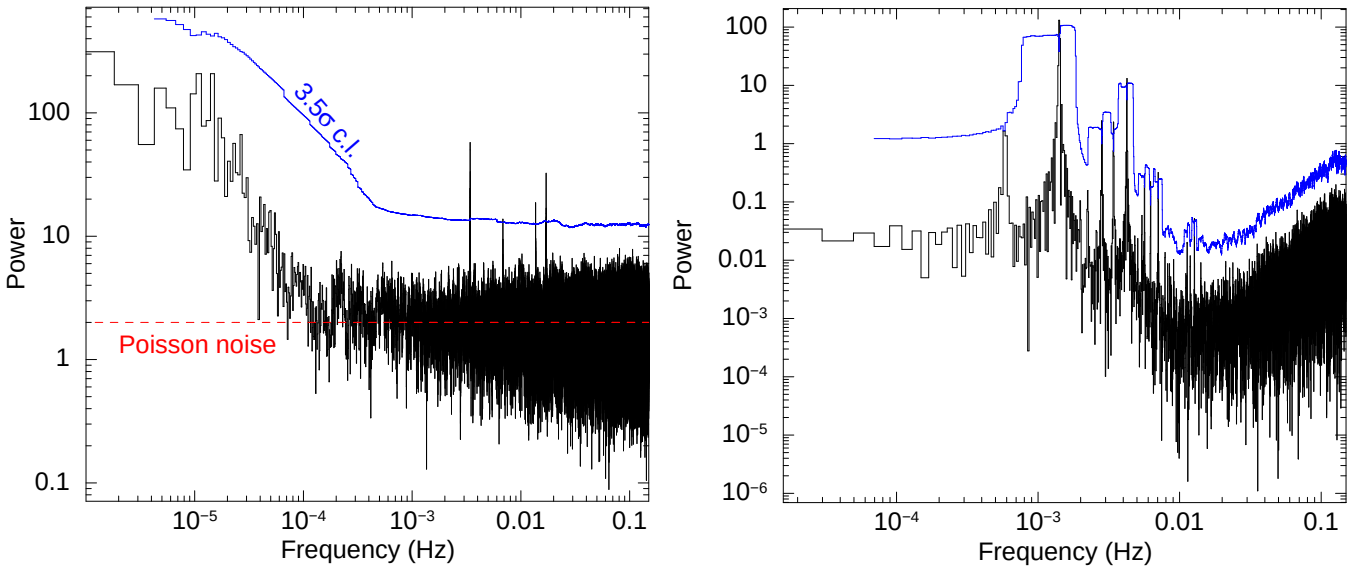

Figure 1. Left panel: Power spectrum density of the 292 s-signal transient pulsar CXOU J005048.0–731817 in the SMC. The solid blue line indicates the 3.5σ detection threshold normalised to the number of independent Fourier frequencies as described in Section 2 and obtained by means of the algorithm described in Israel & Stella (1996). The corresponding Poissonian noise level, according to the Leahy normalization (Leahy et al. 1983), is marked by the stepped red line. In this example a non Poissonian noise component, often referred as red-noise, is evident below 10^{-4} Hz when the power estimates start deviating from the Poissonian noise level. Right panel: As in the first panel, but for the time series of the effective area within the source extraction region as derived with the CIAO DITHER_REGION task.

which presents a statistical tool that can be employed for automatic screening of peaks in PSD obtained by means of fast Fourier Transform (FFT). For each PSD, the algorithm infers a smoothed continuum model by maximizing the Kolmogorov–Smirnov probability that the power spectrum obtained by the ratio between the original one and the smoothed continuum is distributed as a χ^2 with $2N$ degrees of freedom (dof), where N is the number of averaged power spectra (in general, in our project $N = 1$). In this way, it is possible to take into account statistically any non-Poissonian component and set a peak detection threshold which is frequency dependent. The left panel of Fig 1 shows an example of how the CATS @ BAR algorithm automatically sets the detection threshold based on the underlying spectral continuum and records the peaks above the threshold itself. For the project, we set a 3.5σ detection threshold assuming a number of trials equal to the number of FFT frequencies in each PSD.

In principle, the number of trial periods that one should consider is the total number of Fourier frequencies in all the FFTs carried out in the whole project. However, there are two main reasons why we did not abide by this precept. One is that the total number of searched sources and Fourier frequencies will be unknown until the end of the project. The second is that there is a good number of sources which have been observed more than once with *Chandra* and/or *XMM–Newton* (or with other missions). Thus, we preferred to pre-screen the candidate signals based solely on the statistical properties of each individual time series so to leave open the possibility to check later for the recurrence of the same signal within the CATS @ BAR project or for confirmations from data from other missions (mainly *XMM–Newton*, *Swift*, *ASCA*, and *ROSAT*). *A posteriori*, this approach proved to be rather efficient, with about 10 signals confirmed by further *Chandra* pointings carried out during the 15 years interval of our project, and about 15 signals confirmed by data from other missions.

The process described above was implemented in a pipeline which, using tools of the *Chandra* Interactive Analysis of Observations (CIAO; Fruscione et al. 2006) software package, retrieves the relevant ACIS data, detects the sources, extracts the event list files for each object, applies barycentric correction to the event times, checks for the presence of significant (source intrinsic) signals, and, when signals are found, infers their main properties. In particular, we used the CIAO releases from 4.4 to 4.8 (as the project started in 2012 June); the task AXBARY was used for the barycentrization, the tasks ARDLIB, MKINSTMAP, MKEXPMAP, and MAKEPSFMAP, for constructing the exposure and point-spread function maps, and WAVDETECT for the source detection. For the latter, we considered five wavelet detection scales (1, 2, 4, 8, and 16 pixels), and the default value for the source pixel threshold (SIGTHRESH parameter set to 10^{-6}). We notice that the choice of the latter parameters essentially does not impact the results of the project, since we are interested only in relatively 'bright' point-like sources, with at least 50 counts. This minimum number of counts is dictated by the intrinsic capability of the FFT to detect a 100% modulated signal above a 3σ threshold level. Finally, each source event list was extracted from the the 3σ-distribution region determined by WAVDETECT. Besides our codes and CIAO, for the timing analysis we also made use of a number of HEASOFT tools (Blackburn 1995), such as POWSPEC, LCURVE, EFSEARCH, and EFOLD.

Particular attention was paid to the presence of instrumental signals originated by the spacecraft dithering (see also Section 5). A first check is automatically performed by the CATS @ BAR pipeline every time a significant peak is recorded. The procedure is based on the CIAO task DITHER_REGION[3] and checks whether an artificial signal is present in the time series due to the variation of the effective area within the source extraction region. The right panel of Fig. 1 shows an example of a FFT of the time variation of the effective area (as for the FFT in the left panel, the solid blue line marks the 3.5σ detection threshold). In the example, the high-

[3] See http://cxc.harvard.edu/ciao/ahelp/dither_region.html.

est peak corresponds to the well-known ACIS dithering period of 707 s followed by several higher harmonics. The comparison between the spectra, as in the example given in the two panels of Fig. 1, offers to us an objective tool to reject or validate a candidate signal. Additionally, we also inspected the PSD computed from time series of photons accumulated in background regions around or close to each new pulsator (the size and shape of the background region depend from case to case) to check for the presence of peaks consistent with the detected signal.

As of 2015 December 31, we extracted about 430 000 time series from sources with more than 10 counts (after background subtraction); $\sim$190 000 of them have more than 50 counts and their PSDs were searched for significant peaks. At the time of writing, the total number of searched Fourier frequencies was about 4.3×10^9. After a detailed screening, we obtained a final sample of 41 (42) new X–ray pulsators (signals), which are listed in Table 1. For completeness we also list in Table A1 the identification number of all the data sets we used for the analysis. None of the recorded spurious signals falls at the frequency of those periods. The above reported numbers make CATS @ BAR the largest search for signals carried out so far in soft X-rays. Moreover, since the *Chandra* mission is still operative, CATS @ BAR has to be considered a living project: every 1–3 months, the pipeline will be applied to the new public data sets. Based on the results obtained so far, we expect to find about three new pulsators every year.

It is worth emphasizing that the FFT is particularly efficient when dealing with relatively high-statistics time series and/or strong signals. Alternative timing tools, such as periodograms based on the Z_n^2 test (where n stands for the number of the assumed harmonics of the signal) are better suited for the search of faint signals, or strong signals in low-statistics time series, and/or non sinusoidal signals (Buccheri et al. 1983). However, any periodogram algorithm approach suffers from the known problem related to the variable period resolution over the searched period interval. In this respect, the Z_n^2 is better suited when the search is carried out over a relatively narrow period interval (about one order of magnitude). A Z_n^2-based algorithm able to deal with at least four order of magnitudes in periods with a variable period resolution will be applied in the future to the whole sample of 430 000 *Chandra* time series.

3 *XMM–Newton* ARCHIVAL DATA

For each pulsator, when available, we also retrieved, reduced and analysed the relevant *XMM–Newton* archival data of the European Photon Imaging Camera (EPIC). Raw data were reprocessed by means of the Science Analysis Software (SAS, version between 12.0 and 14.0). Data were filtered for episodes of flaring particle background and the times affected by these events were excluded from the analysis. Source photons were extracted from circles with radius of $40''$ or less, depending on the presence of nearby sources and/or background issues and/or the distance from the CCD edges. EPIC background even lists were extracted from source-free regions, the sizes and shapes of which were dictated by nearby sources or background matters. Photon arrival times were converted to the Solar system barycenter using the task BARYCEN using the source coordinates as inferred from the *Chandra* pointings. The ancillary response files and the spectral redistribution matrices for the spectral analysis were generated with ARFGEN and RMFGEN, respectively.

4 CATALOGUE

The main properties of the newly identified *Chandra* ACIS pulsators, together with their signals, are listed in Table 1. The columns report the following quantities/values: (1) The name of the source, where the prefix CXO is used for sources listed in the *Chandra* Source Catalog[4] version 1.1 (CSC; Evans et al. 2010), while CXOU for yet uncatalogued sources; (2,3) Right ascension and declination (J2000); (4) The Galactic latitude; (5) The period of the detected signal; (6) a flag, which summarizes the statistical robustness of the detection (see below for the detailed explanation); (7) The flux of the source or, for variable sources, the flux interval within which the pulsations have been detected; (8) Quantity of Chandra and XMM-Newton observations; (9) Any further relevant information. In some particular cases, we added a section to clarify the possible classification or report on noteworthy facts. The source name and coordinates (columns 1–3) are those in the CSC for catalogued objects (CXO prefix), and the outcomes of the WAVDETECT task for the uncatalogued objects (CXOU prefix).

The periods and their uncertainties in column (5) were inferred in different ways, using case-by-case the technique deemed more appropriate for the data sets available for a source. Depending on the number of observations, their length and count statistics, the periods were determined by either a phase-fitting analysis, a folding analysis, a Z_n^2 test, or a fit with one or more sinusoidal functions. In many cases, due to poor statistics or low number of sampled cycles, we are not able to test if the correct periods are the ones detected or twice these values (as sometimes occurs in CVs). The pulsed fraction is defined as: $PF \equiv (F_{\rm max} - F_{\rm min})/(F_{\rm max} + F_{\rm min})$, where $F_{\rm max}$ and $F_{\rm min}$ are the observed count rates at the peak and at the minimum of the pulse[5].

Three different classes of robustness were defined and one has been assigned to each signal (column 6). The flags are defined as follow. Three asterisks (***) identify an extremely robust signal, which has been detected in more than one data set. Two asterisks (**) indicate a signal detected in only one dataset (the only one available for the given source), but at a high confidence level (above 5σ). Finally, one asterisk (*) is assigned at those signals detected either at a relatively low confidence level (in between 3.5σ and 5σ), or only in one dataset out of two or more observations. Although the latter group of (*) signals might be considered less reliable, we note that a large fraction, about 30%, of the signals first flagged (*) or (**) were later upgraded to the flag (***) after the analysis of further archival or follow-up X-ray observations. This group may also include transient sources.

The values in column 7 are observed fluxes in the 0.5–10 keV, as measured from background-subtracted source spectra, which were created with the CIAO's SPECEXTRACT task. Energy channels were grouped so to have at least 15 counts in each new energy bin. All bins consistent with zero counts after background subtraction were removed before fitting the data. For simplicity and uniformity, we always used a simple absorbed power-law model, which in most cases provided an acceptable fit to the data.

The last column of Table 1 (9) includes references and information deemed interesting for the nature of the source and/or the signal. Among others, are the Galactic latitude; possible associations with star clusters, or galaxies, or coincidence with sources detected from other missions; relevant properties inferred from the

[4] See http://cxc.harvard.edu/csc/ for more details.
[5] See http://www.physics.mcgill.ca/∼aarchiba/pulsed-flux-CASCA-07.pdf for a comparison among different definitions of pulsed fraction.

Table 1. CATS catalogue. An updated online version of the Table is maintained at http://www.oa-roma.inaf.it/HEAG/catsatbar/ .

Name	R.A. (hh mm ss.s)	Dec. (° ′ ″)	b (°)	Period[a] (s)	Flag[b]	Flux[c] (erg cm^{-2} s^{-1})	XMM/Chandra[d]	Comments[e,f]
CXO J002415.9–720436	00 24 15.9	–72 04 36.4	–44.9	8 649(1)	***	0.5–0.8	C(16)	E, 47 Tuc
CXOU J004814.1–731003	00 48 14.1	–73 10 03.7	–44.0	50.669(1)	***	4–45	C(1)/X(2)	T, HMXB, SMC (SXP 25.5, SXP 51,XMMU J004814.1–731003)
CXOU J005048.0–731817	00 50 48.0	–73 18 18.2	–43.8	292.784(5)	***	5–22	C(6)	T, SMC, HMXB (RX J0058.2–7231, XTE J0051–727), O (e. l.), [1]
CXOU J005440.5–374320	00 54 40.5	–37 43 20.2	–79.4	21 180(485)	*	0.9	C(1)	T, NGC 300, perhaps a foreground CV
CXOU J005758.4–722229	00 57 58.4	–72 22 29.5	–44.7	7.918 07(5)	***	4–20	C(2)/X(1)	T, HMXB, SMC, O (e.l.), [2]
CXO J021950.4+570518	02 19 50.5	+57 05 18.2	–3.7	4 782(5)	***	0.3–0.6	C(4)/X(1)	Pst, h Persei (NGC 869), O (e. l.)
CXOU J055930.5–523833	05 59 30.5	–52 38 33.5	–28.9	21 668(200)	*	0.2	C(3)	CV?
CXOU J063805.3–801854	06 38 05.3	–80 18 54.1	–27.3	13 151(330)	**	4	C(1)	CV?
CXOU J091539.0–495312	09 15 39.0	–49 53 12.9	–49.9	55.97(1)	*	1.2	C(1)	transient
CXOU J111133.7–603723	11 11 33.7	–60 37 23.0	-60.6	9 766.8(5)	***	1.2	C(7)/X(1)	O (3 possible counterparts)
CXOU J112347.4–591834	11 23 47.4	–59 18 34.2	–59.3	1 525.92(6)	***	2.8–5.5	C(7)/X(2)	near SNR G292.0+1.8
CXO J123030.3+413853	12 30 30.3	+41 38 53.1	+74.9	23 148(396)	***	0.2–1	C(5)/X(2)	NGC 4490, BH–WR candidate [3]
CXOU J123823.4–682207	12 38 23.4	–68 22 07.0	–5.5	5 065(40)	*	2.1	C(1)	
CXOU J141332.9–651756	14 13 32.9	–65 17 56.5	–3.8	6 377(4)	***	0.4–0.6	C(2)/X(1)	CV (Polar?) [4]
CXO J141430.1–651621	14 14 30.1	–65 16 23.3	–3.8	6 120(2)	***	1.1–1.4	C(4)/X(1)	IP [4]
				64 200(500)	**			Same source as above. Long period, likely of orbital origin
CXOU J153539.8–503501	15 35 39.8	–50 35 01.4	–4.2	12 334(567)	**	9	C(1)	NGC 5946
CXO J161437.8–222723	16 14 37.9	–22 27 23.7	+20.2	5 671(137)	**	0.5	C(1)	T, CV?, 100% PF
CXOU J163855.1–470145	16 38 55.1	–47 01 45.8	–0.1	5 684(40)	***	0.9	C(2)/X(1)	NS?, Norma Arm?, 100% PF
CXO J170113.3+640757	17 01 13.3	+64 07 58.5	+36.2	5 674(1)	***	0.3	C(9)/X(1)	100% PF, O (e.l.)
CXO J170214.7–295933	17 02 14.7	–29 59 33.6	+7.2	11 467(500)	***	0.2	C(6)	Pst, 100% PF
CXO J170227.3–484507	17 02 27.4	–48 45 07.1	–4.3	3 080(40)	***	0.7–1.4	C(2)/X(2)	Pst
CXO J171004.6–321205	17 10 04.6	–32 12 05.5	+4.5	4 990(15)	***	0.9–2.8	C(2)	∼100% PF
CXOU J173037.7–212633	17 30 37.7	–21 26 33.0	+4.6	5 059.40(7)	***	0.3	C(9)	near Kepler SNR
CXOU J173113.7–212552	17 31 13.7	–21 25 52.1	+6.7	15 532(64)	*	11	C(2)	Pst, O (e. l.)
CXO J173359.0–220614	17 33 59.1	–22 06 14.1	+5.8	4 745(23)	*	0.4	C(1)	O
CXOU J174042.3–534029	17 40 42.3	–53 40 28.9	–12.0	21 134(33)	***	5.7	C(5)	in NGC 6397
CXO J174245.1–293455	17 42 45.1	–29 34 55.4	+0.2	12 220(1164)	*	0.5	C(2)	Galactic bulge
CXO J174638.0–285325	17 46 38.0	–28 53 25.9	–0.2	21 887(538)	***	2.0	C(4)/X(2)	Galactic bulge, CV, O (e.l.)
CXOU J174811.0–244930	17 48 10.1	–24 49 03.0	+1.6	5 017(19)	***	0.4	C(2)	Terzan 5, ∼100% PF
CXOU J180839.8–274131	18 08 39.8	–27 41 31.6	–9.9	854(14)	*	27	C(1)	O (e. l.; OGLE source, 0.28 d)
CXO J180900.0–435039	18 09 00.1	–43 50 40.0	–11.4	5 842(115)	*	1.6	C(1)	NGC 6541
CXOU J181516.4–270851	18 15 16.4	–27 08 51.6	–4.8	472(1)	**	4.5	C(2)	O ?
CXOU J181924.1–170607	18 19 24.1	–17 06 07.2	–0.9	407.8(1)	***	8.5–46	C(1)/X(3)	V, O (e.l.), [5,6]
CXO J184441.7–030549	18 44 41.7	–03 05 49.4	+0.1	6 366(236)	**	0.4-11	C(3)/X(3)	V
CXOU J185415.8–085641	18 54 15.8	–08 56 41.2	–4.7	5 790(208)	*	0.6	C(1)	
CXOU J191043.7+091629	19 10 43.7	+09 16 29.2	–0.02	36 204(109)	**	4–24	C(2)/X(1)	V, HMXB, AX J1910.7+0917, INTEGRAL, $K = 11.8$
CXO J193437.8+302524	19 34 37.8	+30 25 24.4	+5.0	5 906(200)	***	1.8	C(1)/X(1)	O (e.l.)
CXOU J204734.8+300105	20 47 34.8	+30 01 05.2	–8.4	6 097(82)	***	9–21	C(1)/X(1)	E, Polar ?, O (e.l.)
CXOU J215447.8+623155	21 54 47.8	+62 31 55.0	+6.3	9 933(10)	***	1.6	C(4)	O (e.l.)
CXOU J215544.5+380116	21 55 44.5	+38 01 16.3	–13.0	14 090(43)	**	0.3	C(2)	O (e.l.)
CXOU J225355.1+624336	22 53 55.1	+62 43 36.8	+2.9	46.673 66(4)	***	20–50	C(5)/X(1)	HMXB, O (e. l.), [8]

Table 1 – *continued*

Name	R.A. (hh mm ss.s)	Dec. (° ′ ″)	b (°)	Period[a] (s)	Flag[b]	Flux[c] (erg cm^{-2} s^{-1})	XMM/Chandra[d]	Comments[e,f]
Sources with signals published by other groups while the project was on-going and/or with rough estimate of the periods								
CXO J165334.4–414423	16 53 34.4	–41 44 23.8	+1.3	5 820(20)	***	0.2	C(1)/X(6)	CV, [9]
CXO J174728.1–321443	17 47 28.1	–32 14 43.9	–2.1	4 831(2)	***	0.4–9.5	C(3)/X(1)	V, [7]
CXO J182531.4–144036	18 25 31.5	–14 40 36.5	–1.1	781(1)	***	14	C(2)/X(1)	[7], CV ?
CXO J191404.2+095258	19 14 04.2	+09 52 58.4	–0.5	5 937(219)	*	280	C(1)/X(1)	HMXB, IGR J19140+0951, $P\mathrm{orb} = 13.55\,\mathrm{d}$, $K\mathrm{s} = 8.7$, [10]

[a] The uncertainty is given at a 90% confidence level.

[b] The number of stars indicates detection confidence as follows: *** Multiple detection of the same signal (either with *Chandra* or with other missions); ** Single high confidence ($>10\sigma$) detection; * Single detection (above 3.5σ). See also Section 4.

[c] Observed 0.5–10 keV flux in units of 10^{-13} erg cm^{-2} s^{-1} for a power-law fit. A range of values indicates different values measured in the *Chandra* observations used for the timing analysis.

[d] Number of useful *Chandra* and *XMM–Newton* pointings used to evaluate the signal/source parameters. We counted only those observations where the signal was detected or those with no detection but 3σ pulsed fraction upper limits smaller than that of the modulation were inferred. We also counted observations where the source was not detected at a comparable or lower flux level with respect to the original detection level or detected at a significantly different flux level.

[e] E: eclipsing; T: transient: the source was not detected in some observations with *Chandra* or other missions; Pst: persistent: the flux did not vary by more than a factor of 5 in the observations we considered; V: variable: we measured flux variations larger than a factor of 5; O: optical counterpart or association. Question marks denote tentative identifications or associations.

[f] References: [1] Esposito et al. (2013c); [2] Bartlett et al. (2016); [3] Esposito et al. (2013a); [4] Esposito et al. (2015b); [5] Nichelli et al. (2011); [6] Farrell et al. (2015); [7] Muno et al. (2008); [8] Esposito et al. (2013b); [9] Lin et al. (2014); [10] Sidoli et al. (2016).

X-ray data (transient, eclipsing, persistent, or variable sources) or optical data (both from catalogues or follow-up observations).

For a subsample of 10 new X-ray pulsators, we obtained X-ray follow-up observations with *Chandra*, *Swift*, or *XMM–Newton*, seven of which were already carried out. Similarly, in the latest four years, we performed optical spectroscopic follow-up for about half the sources. In those cases where a good optical counterpart candidate was found, based on the positional coincidence and the detection of emission lines (e.l.) in the spectrum, we included the piece of information in column 9 as 'O(e.l.)'. More details and results from X-ray and optical follow-up observations are already published for some sources (the references are provided in column 9 and in the paragraphs on individual sources) and for others will be included in a forthcoming paper (Israel et al. in preparation).

In column 9 we used the following acronyms: NS, neutron star; BH, black hole; WR, Wolf–Rayet star; SNR, supernova remnant; SMC, Small Magellanic Cloud. Most sources are expected to be CVs or HMXBs; in general we favour a CV identification when the source is far from the Galactic plane (high or low Galactic latitude b) and/or the luminosity appears to be low ($<10^{32}$ erg s^{-1}) and/or there are possible associations with globular clusters or faint optical counterparts; we favour an HMXB nature when a period variation ($\dot{P}$) is measured and/or there is a possible bright optical counterpart. The pulse profiles of detected pulsators are shown in Fig. 2 and 3 together with their inferred periods and pulsed fractions.

An on-line version of the CATS @ BAR catalogue is maintained at http://www.oa-roma.inaf.it/HEAG/catsatbar/ . It will include new sources detected in the future and updated information.

4.1 Individual sources

The signals reported for CXO J165334.4–414423, CXOU J181924.1–170607, CXO J182531.4–144036 and CXO J174728.1–321443 were independently discovered in other projects using *XMM–Newton* or *Chandra* data (Lin et al. 2014; Farrell et al. 2015; Muno et al. 2008). We listed them even so, because either we discovered them before their publication (for the first two cases; Lin et al. 2014; Farrell et al. 2015) or because our analysis led us to different conclusions (in the other instances; Farrell et al. 2015; Muno et al. 2008).

4.1.1 CXO J002415.9–720436

This source is possibly part of the globular cluster 47 Tuc, which was observed with *Chandra* many times (e.g. Grindlay et al. 2001; Edmonds et al. 2003a,b; Heinke et al. 2005b; Heinke, Grindlay, & Edmonds 2005a). The timing and spectral parameters in Table 1 were inferred from observations 953, 955, and 2735–8. Although the signal was originally detected at about 4 325 s, the study of the pulse shape revealed that the correct period is about 8 650 s. In fact, when folded at the latter period, the pulse profile is asymmetric and shows a total eclipse lasting for about 8 minutes (Fig. 2). Edmonds et al. (2003a) proposed an X-ray period of 6.287 h, which is not confirmed by our analysis. The length of the period and the presence of a total eclipse strongly favour a CV interpretation, as it was proposed by Edmonds et al. (2003a).

4.1.2 CXOU J004814.1–731003

The power spectrum shows one highly-significant signal at 51 s plus its harmonic at 25.5 s. Moreover, the *Chandra* position is consistent with that of XMMU J004814.1–731003, a 25.5-s Be/XRB pulsar (Haberl et al. 2008b). Our findings strongly suggest that SXP 25.5 (Lamb et al. 2002), SXP 51 (Galache et al. 2008), XMMU J004814.1–731003, and CXOU J004814.1-731003 are all the same source, and its true period is $\sim$51 s.

4.1.3 CXOU J005048.0–731817

CXOU J005048.0–731817 is a transient HMXB pulsar in the SMC. In 2010 April–May, this source underwent a long-lived ($\sim$20 d) outburst, during which the luminosity increased by about two orders of magnitude (up to $\sim 1.2\times10^{36}$ erg s^{-1}). The event was fortuitously sampled by 7 *Chandra* observations and the source was serendipitously detected in its quiescent state, at a luminosity of $\sim 10^{34}$ erg s^{-1}, in other 15 *Chandra* pointings from 2002 October to 2010 June. The fact that, despite all this, the source went unnoticed in the *Chandra* data for years, even in campaigns focussed on the study of HMXBs in the SMC, testifies to the importance of systematic searches for periodic signals.

Detailed analysis of this transient pulsar was reported in Esposito et al. (2013c). Here we just make two remarks. Firstly, we note that CXOU J0050 is a different object from the SMC pulsar RX J0058.2–7231 (Haberl, Eger, & Pietsch 2008a), which has a similar period ($\sim$291 s) but is located about 1° away. However, it is unclear whether CXOU J0050 or RX J0058.2–7231, as proposed by Haberl et al. (2008a), is responsible for the RXTE detection of the 293 s signal tentatively catalogued as SXP 293 (XTE J0051–727; Corbet et al. 2004b), whose uncertain position is consistent with both objects (Galache et al. 2008). Secondly, the analysis of archival spectra of the optical counterpart of CXOU J0050 taken in September 2007 with the 3.6-m ESO telescope, allowed us to refine the spectral classification, which resulted to be a O9–B0 (more likely an O9) IV–V class spectral-type star.

4.1.4 CXOU J005758.4–722229

Detailed analysis of this source will appear in Bartlett et al. (2016).

4.1.5 CXO J021950.4+570518

The presence of a faint ($V > 20$) counterpart in the X-ray error circle and a luminosity of $(2-4)\times10^{30}$ erg s^{-1} (assuming a distance to NGC 869 of 2.4 kpc; Currie et al. 2009) suggest a CV.

4.1.6 CXOU J063805.3–801854

A bright star ($B = 16.3$, $R = 15.7$; USNO-B1.0 0096-0020652) is consistent with the X-ray error circle.

4.1.7 CXO J123030.3+413853

CXO J123030.3+413853 is located in the low-metallicity spiral galaxy NGC 4490, which is interacting with the smaller irregular NGC 4485. In Esposito et al. (2013a), we interpreted its strong modulation at $\sim$6.4 h ($\sim$90% pulsed fraction, confirmed also by *XMM–Newton* data) as an orbital period and, considering the morphology of the folded light curve and the maximum peak X-ray

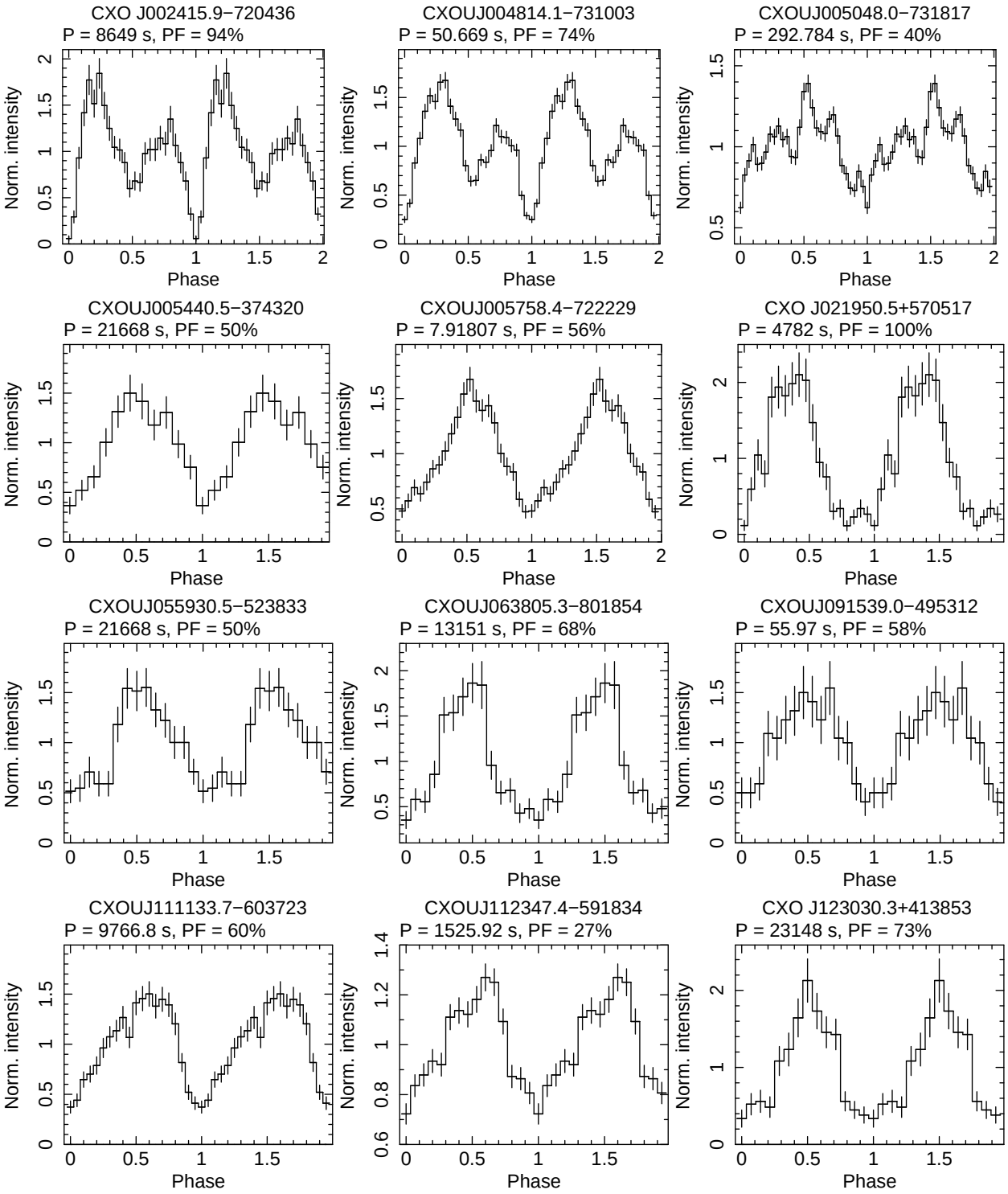

Figure 2. CATS pulse profiles. The source, as well as the period used to fold the data and the pulsed fraction, are indicated in each panel.

luminosity of $\approx 2 \times 10^{39}$ erg s^{-1} (for $d = 8$ Mpc), we proposed the source as a BH HMXB with a Wolf–Rayet (WR) star donor.

Besides their rarity and evolutionary interest, these systems are particularly interesting because they are precursors of NS–BH and BH–BH binaries, which may merge emitting gravitational waves and creating a more massive BH (Abbott et al. 2016). In Esposito et al. (2015b), we derived from the current sample of BH–WR candidates (7 objects, in four of which the WR counterpart has been securely identified) an upper limit to the detection rate of stellar BH–BH mergers with Advanced LIGO and Virgo of $\sim$16 yr^{-1}

4.1.8 CXOU J141332.9–651756 and CXO J141430.1–651621

Periodic signals from these sources were discovered in a long exposure of the Circinus galaxy (ESO 97–G13). CXO J141430.1–651621 is more than 2 arcmin out of the border of the Circi-

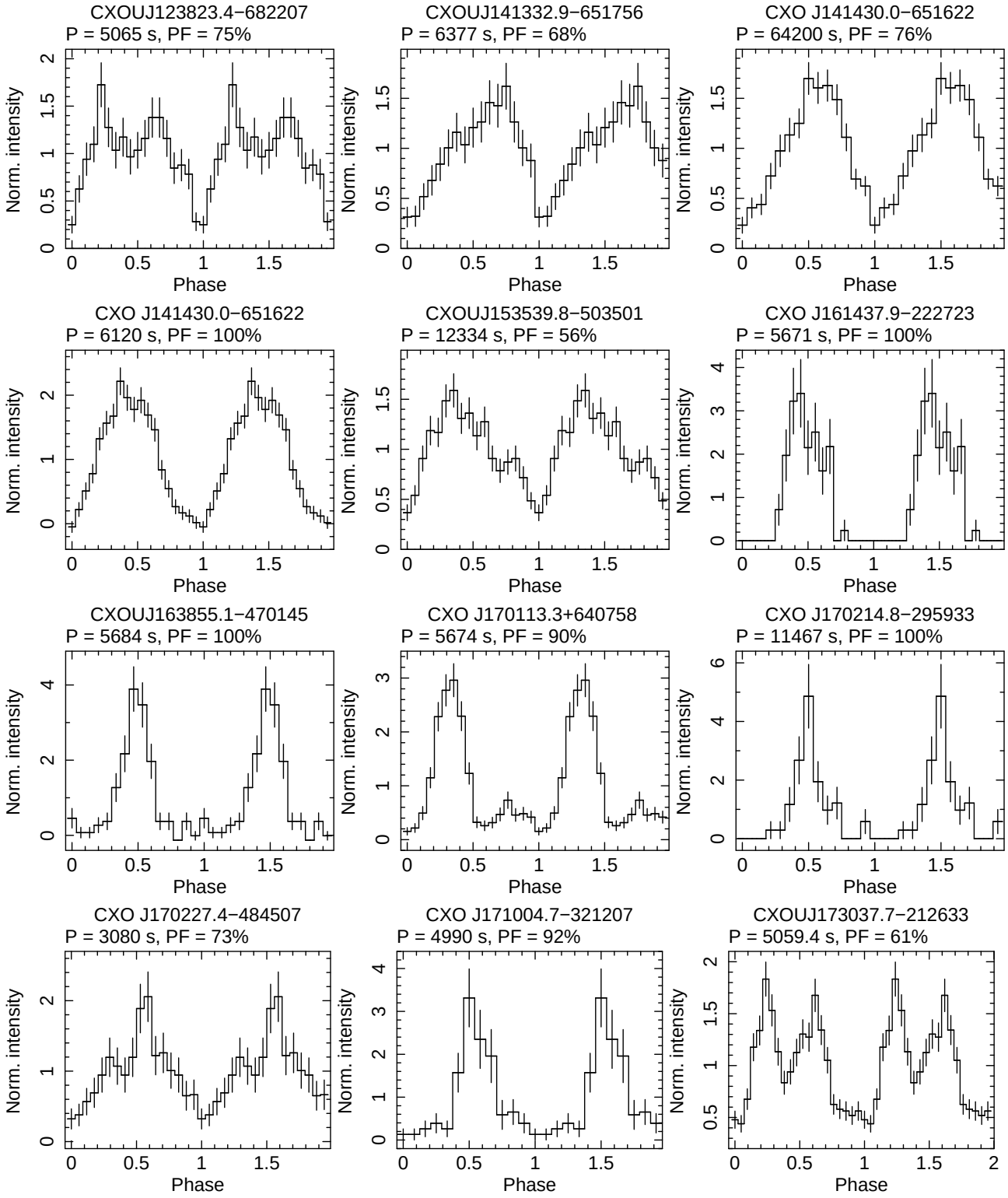

Figure 2 – *continued*

nus galaxy and therefore an association is ruled out. A spin period of 1.7 h and an orbital period of 17.8 h pin down the source a CV of the IP type. Its X-ray spectrum can be modelled by a power law with photon index $\Gamma \simeq 1.4$ and the flux of $\approx 1 \times 10^{-13}$ erg cm^{-2} s^{-1} shows ≈50 per cent variability on time-scales of weeks–years. The typical luminosity of IPs and the nondetection of the optical counterpart suggest a distance larger than ∼5 kpc (Esposito et al. 2015b). Albeit at ∼3.5 arcmin from the nucleus, CXOU J141332.9–651756 appears inside the Circinus galaxy. However, the absorption column, which is much smaller than the total Galactic density in that direction, argues against an extragalactic source. Indeed, the probability of a foreground

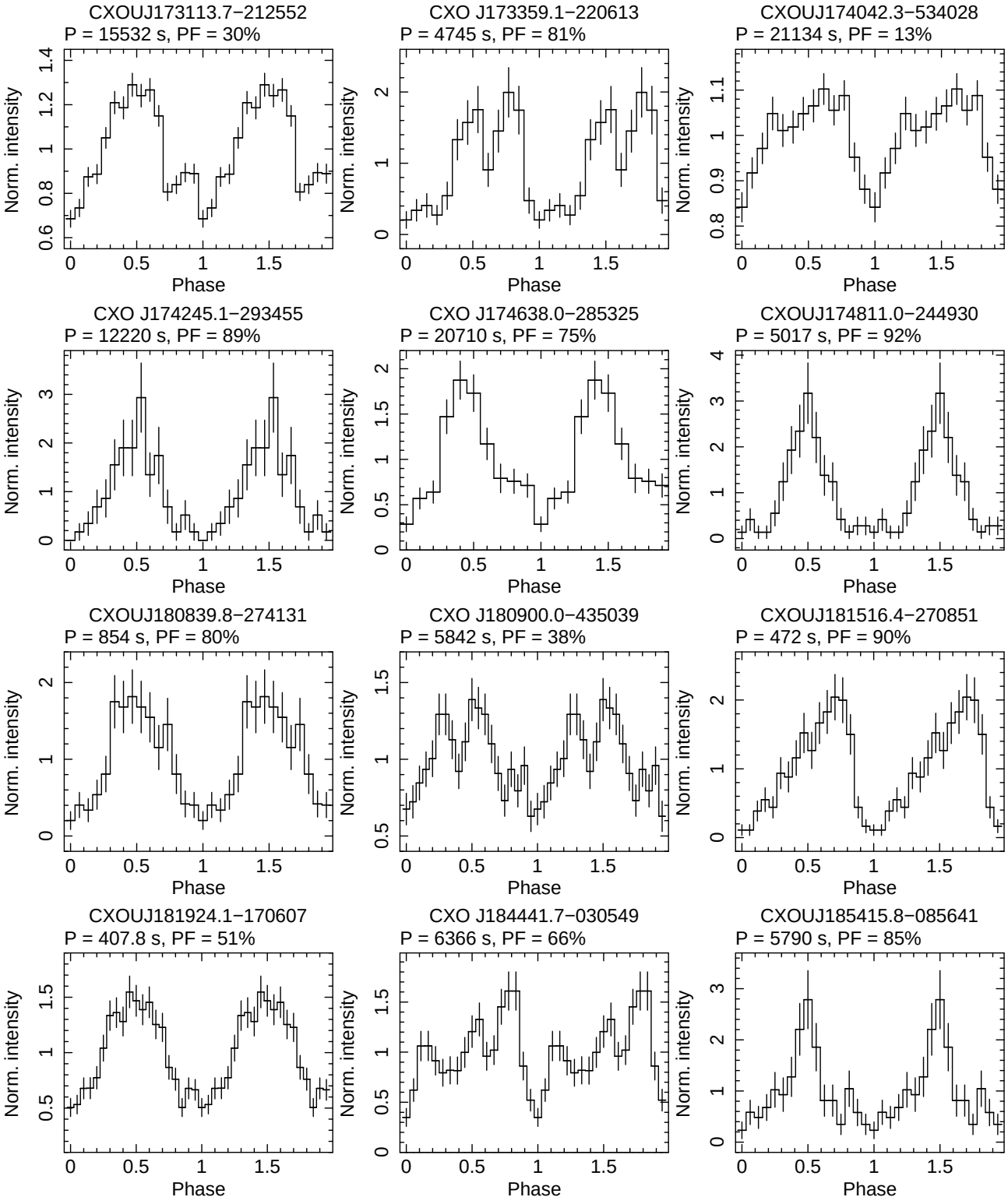

Figure 2 – *continued*

Galactic X-ray source is substantial (≈10 per cent, as estimated from the cumulative Galactic X-ray source density versus flux distribution from the *Chandra* Multi-wavelength Plane survey by van den Berg et al. 2012). The modulation period is 1.8 h and the emission (flux of $\approx 5 \times 10^{-14}$ erg cm^{-2} s^{-1}, with ≈50 per cent variations on weekly/yearly scales) can be described by a power law with $\Gamma \simeq 0.9$. CXOU J141332.9–651756 is probably a (Galactic) magnetic cataclysmic variable, probably of the polar type (Esposito et al. 2015b). Assuming that the companion is a M5V star (or similar), the nondetection of its optical counterpart implies $d \gtrsim 0.7$ kpc; therefore, if the system is within a few kpc, its luminosity is in the normal range for polars.

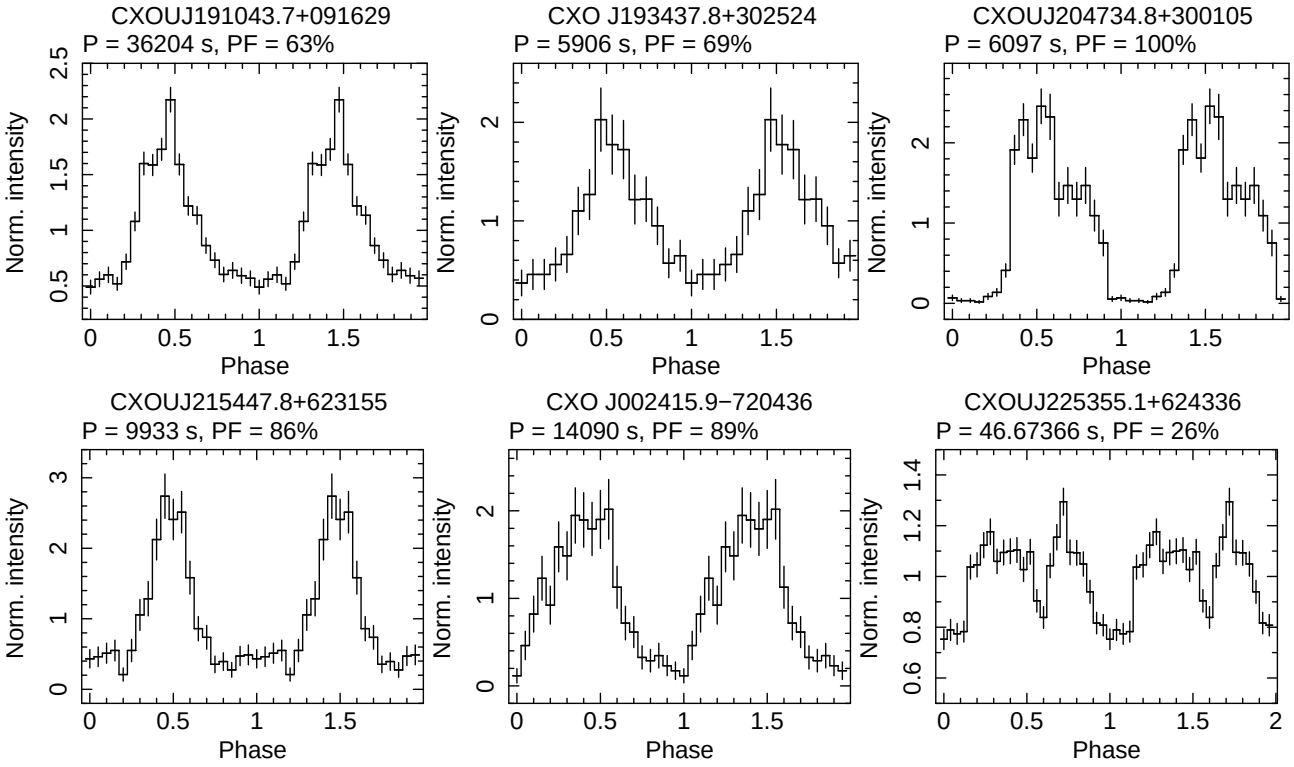

Figure 2 – *continued*

4.1.9 CXOU J153539.8–503501

This source is within the tidal radius of the globular cluster NGC 5946 (Davidge 1995). A possible faint counterpart ($V > 20$) is consistent with its *Chandra* error circle.

4.1.10 CXOU J163855.1–470145

Archival *XMM–Newton* data confirm the modulation at a period of 5 827(19) s, implying a spin-down rate of $8(2) \times 10^{-7}$ s s^{-1}; or 25(8) s yr^{-1}. This suggests that the pulsations reflect the rotation of a NS. Assuming a distance of 10 kpc for the Norma Arm, the luminosity is $\sim 10^{33}$ erg s^{-1}.

4.1.11 CXO J170113.3+640757

Optical spectroscopic follow-up observations led to the identification of an optical counterpart showing H and He emission lines.

4.1.12 CXOU J173113.7–212552

The period was discovered in the *Chandra* obs. 6714, but not in obs. 6716, few days apart. An *XMM–Newton* pointing detected the source, but is too short to confirm the signal (less than 2 cycles are covered). Optical spectroscopic follow-up observations carried out at NOT led to the identification of an optical counterpart showing H and He emission lines.

4.1.13 CXO J174638.0–285325

Koenig et al. (2008) reported on the optical spectroscopy of the likely counterpart of this source as part of the study of the *Chandra* Multiwavelength Plane Survey, ChaMPlane. Based on broad Hα emission line in the spectrum of the $R = 20.2$ magnitudes counterpart and a X-ray to optical flux ratio of 0.07, Koenig et al. (2008) classified this source as a candidate CV. Our discovery of a period of $\sim$6.1 hr supports a CV nature for the new pulsator.

4.1.14 CXO J174728.1–321443

Muno et al. (2008) proposed a modulation around 5 000 s using the same data sets (4566–4567, 2004 March). In an *XMM–Newton* follow-up observation carried out in 2014 August, we measured a period of 4 941(52) s which is, within uncertainties, consistent with the *Chandra* value. *XMM–Newton* caught the source at a much lower flux of $\sim 4 \times 10^{-14}$ erg cm^{-2} s^{-1}, a factor of about 25 fainter.

4.1.15 CXOU J174811.0–244930, CXO J180900.0–435039

These sources are within the tidal radius of the globular cluster Terzan 5 (Lanzoni et al. 2010) and NGC 6541 (Harris 1996), respectively.

4.1.16 CXOU J181924.1–170607

First discovered by our group in *Swift* and *XMM–Newton* datasets (Nichelli et al. 2011), was later rediscovered by Farrell et al. (2015). Optical spectroscopic follow-up observations carried out at NOT led to the identification of a faint optical counterpart showing H and He emission lines. Furthermore, by using all the *Chandra*, *XMM–Newton* and *Swift* archival data, which span over more than 8 years, we inferred a 3σ upper limit on the first period derivative

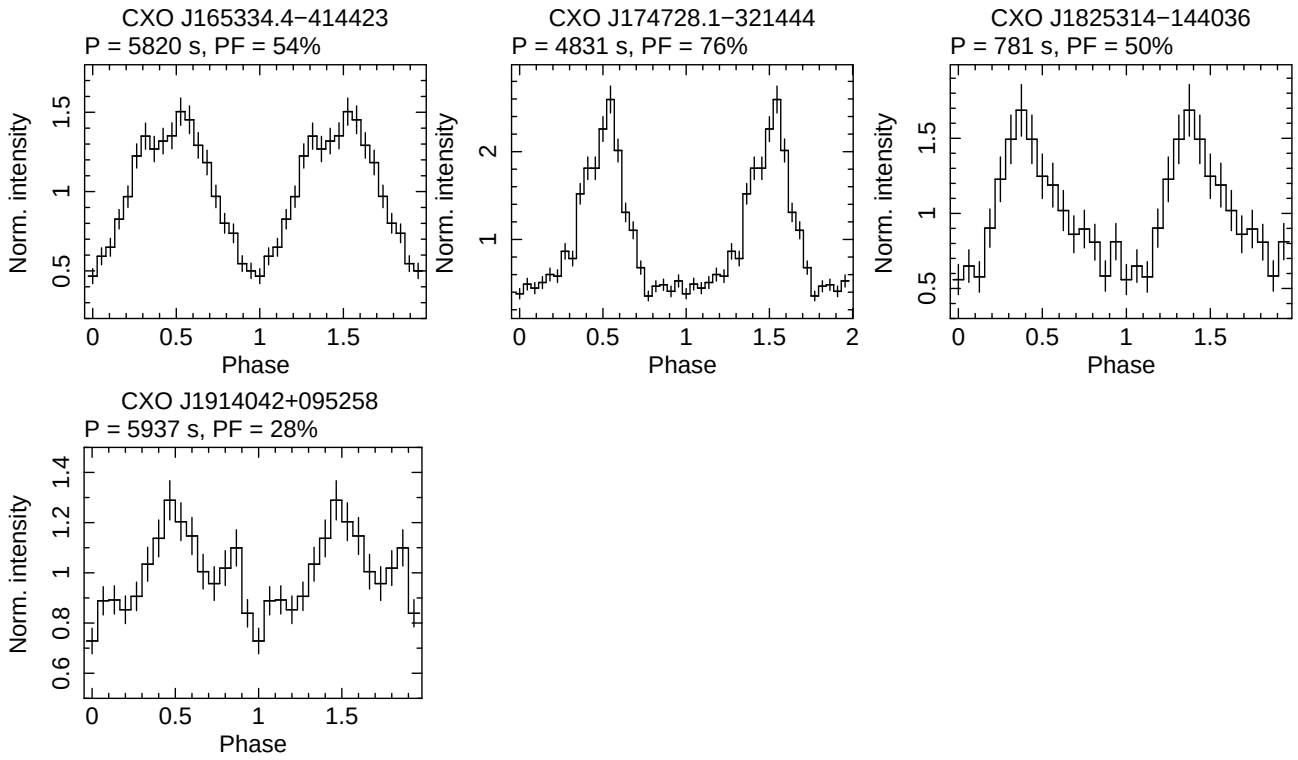

Figure 3. Same as Figure 2 but for the latest three sources in Table 1

of $|\dot{P}| < 10^{-11}$ s s^{-1}. These findings strongly disfavour the scenario of a slow X-ray pulsar in a HMXB (Farrell et al. 2015), while strengthens the CV scenario proposed by Nichelli et al. (2011).

4.1.17 CXO J182531.4–144036

Pulsations at a period of 785(2) s and 5 000 s were first reported by Muno et al. (2008), based on a *XMM–Newton* pointing carried out on 2008 April 10–11, when the source was detected at a flux of $1.9(1) \times 10^{-12}$ erg cm^{-2} s^{-1}(35% larger than in the *Chandra* data). The 5 000 s signal was classified as a likely noise fluctuation. Our detection of 781(s) s pulsations in a 2004 July *Chandra* observation shows that the period did not changed significantly among the two epochs. Additionally, there is evidence for a longer modulation around about 5 000 s in the same *Chandra* dataset. We assigned a *** flag to the 781 s signal.

4.1.18 CXO J191404.2+095258

CXO J191404.2+095258 is the soft X-ray counterpart of IGR J19140+0951, discovered with *INTEGRAL* in 2003 March (Hannikainen et al. 2003). It was identified as an HMXB with orbital period of 13.552(3) d (Corbet et al. 2004b; Wen et al. 2006) and a B0.5 supergiant companion (in't Zand et al. 2004) located at a distance of about 3.6 kpc (Torrejón et al. 2010). It is a very variable source (Corbet et al. 2004a; in't Zand et al. 2004), with an X-ray intensity that can span 3 orders of magnitudes (Sidoli et al. 2016). in't Zand et al. (2004) reported on the hint of a possible modulation at ∼6.5 ks, that needed confirmation. A modulation near that value was indeed found in our project (∼5.9 ks; Table 1). A 1.46 mHz quasi-periodic oscillation was discovered during a recent XMM-Newton observation (Sidoli et al. 2016).

4.1.19 CXO J193437.8+302524, CXOU J204734.8+300105, CXOU J215447.8+623155, CXOU J215544.5+380116

For all these sources, optical spectroscopic follow-up observations led to the identification of optical counterparts showing H and He emission lines.

4.1.20 CXOU J225355.1+624336

We discovered in CXOU J225355.1+624336 a modulation at ∼47 s in a series of *Chandra* observations carried out in 2009. The modulation was recovered also in *Swift* and *ROSAT* data, allowing us to infer an average increasing rate of the period of ∼17 ms per year in 16 years and, therefore, to decipher the signal as the rotation period of an accreting, spinning-down NS (Esposito et al. 2013b).

Follow-up observations at the Nordic Optical Telescope made it possible to classify the NS companion as a B0-1III-Ve (most likely a B1Ve) star at a distance of about 4–5 kpc. The X-ray luminosity of $\sim 3 \times 10^{34}$ erg s^{-1}, steady within a factor of ∼2, suggests that 1RXS J225352.8+624354 is a new member of the subclass of low-luminosity persistent Be/X-ray pulsars similar to X Persei, which have long orbital period ($P_{\rm Orb} \gtrsim 30$ d) and wide and circular orbits ($e < 0.2$).

5 SIGNALS OF INSTRUMENTAL ORIGIN

As a by-product of the project, we collected and analysed all the information related to the spurious signals recorded by the detection algorithm. Fig. 4 shows the sensitivity map as a function of frequency for the CATS signal search. Boundaries are dictated towards low frequencies by the maximum length of a single pointing (one orbit of about 130 ks), and at high frequencies by the readout

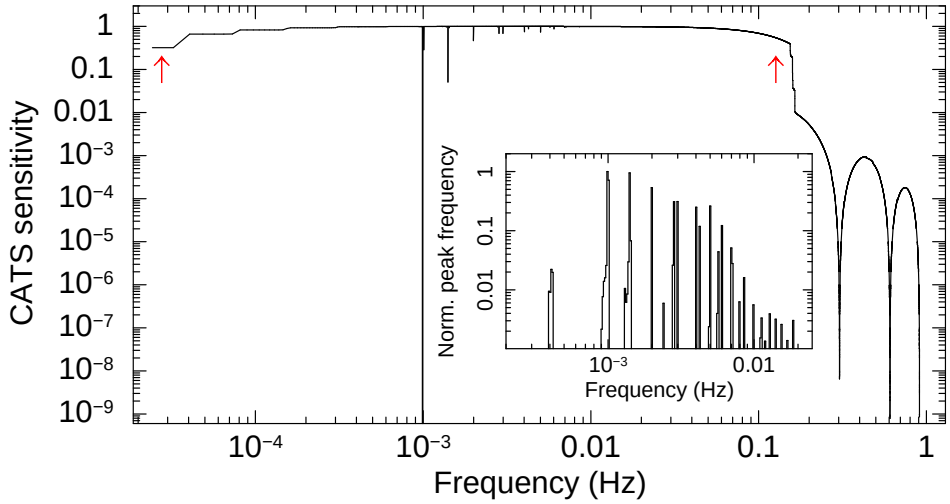

Figure 4. Sensitivity map as a function of frequency for the CATS signal search: drops in the sensitivity are due to the dithering signals (in the 10^{-3}– 10^{-2} Hz interval) and the sampling times (above 0.1 Hz; see Section 5 for details). The red arrows mark the longest and shortest period discovered by the CATS pipeline. In the inset we show the more frequent spurious signals detected by the pipeline during the search, the most prominent being at the dithering frequencies plus many harmonics.

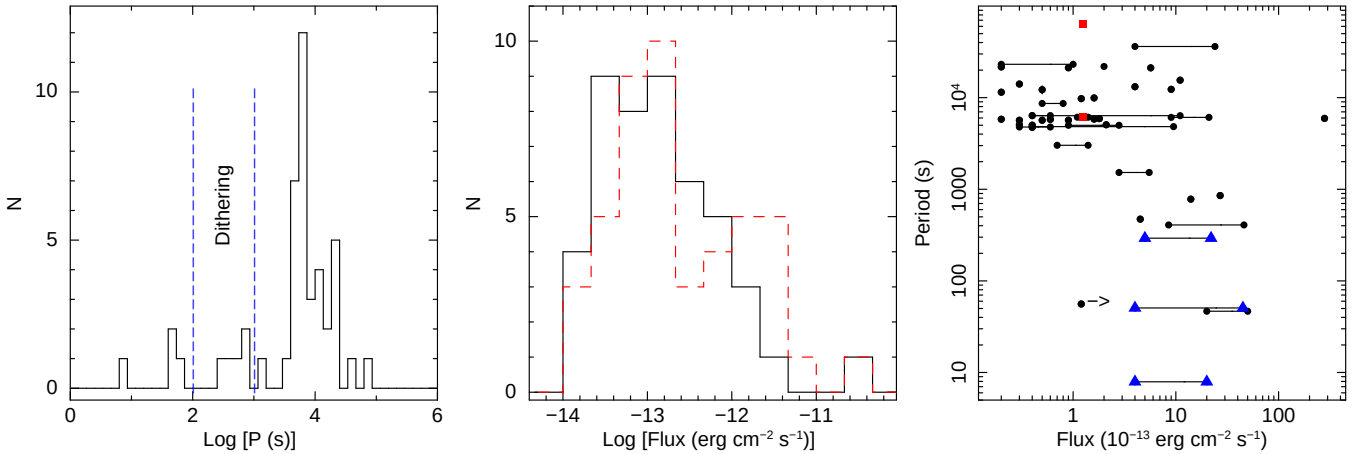

Figure 5. Main properties of the CATS@BAR sample of new X-ray pulsators. From left to the right are shown the period distribution (left panel), the flux distribution (central panel), and the period versus flux plane (right panel), where the solid lines mark the objects detected at different flux levels (the right arrow marks a variable object for which we can rely upon only one dataset), the (blue) triangles corresponds to the transient NSs in the Be X-ray binaries of the SMC, and the (red) squares the spin and orbital periods of the new CV/IP in the field of view of the Circinus galaxy. In the left panel we marked the period interval where the effects of the spacecraft dithering humper the detection of true signals. In the central panel the solid black and the stepped red lines correspond to the flux distributions obtained by assuming the minimum and maximum fluxes of variable objects, respectively.

times of the ACIS. For most observations it is 3.2 s (0.3125 Hz), while in subarray modes it can be from 1/2 to 1/8 of the nominal value; this is reflected by the bumps at high frequency which are due to the corresponding Nyquist frequencies. The sharp drops are produced by the ACIS dithering periods (1 000 s and 707 s) and their harmonics extending up to 0.02 Hz. This is shown in more details in the inset, where we plotted all the detected spurious signals. We notice the presence of a number of additional signals, which are not likely associated to any of the fundamental dithering frequencies but present in some pointings (such as the signal at 4×10^{-4} Hz). The use of the CIAO task DITHER_REGION for each detected signal allowed us to reject these cases (see also Section 2). The red arrows mark the longest and shortest period discovered by the CATS pipeline, namely CXOU J005758.4–722229 (7.9 s) and CXOU J191043.7+091629 (36 204 s, see Table 1).

6 SUMMARY AND CONCLUSIONS

In Figure 5 we present some characteristics of the CATS@BAR selected sample. The first panel shows the period distribution. Although some frequency intervals are affected by the sensitivity issues discussed in Section 5, a clustering around $\log P \simeq 3.8$ (about 6 000 s) is evident. This resembles the period distribution of CV peaking at $\log P \simeq 3.8$ and $\log P \simeq 4.2$ with a gap in between (Knigge et al. 2011). This agrees with the preliminary classification of the sources in Table 1.

It is worth noticing that all the similar projects carried out in the past and briefly overviewed in Section 1 discovered only pulsators with periods above ∼400 s, we also detected pulsators as fast as 8 s. This is partly due to the algorithm employed (mainly LS periodograms and algorithms based on the Z^2 statistics), partly might be due to the likely larger number of pulsators with intrin-

sically longer periods, and partly to the increasingly incidence of spin modulations at short periods. In the latter case, their detection depends on the physical conditions of the accreting object (see below).

The observed flux distribution (in the 0.5–10 keV band) is shown in the second panel of Figure 5. The relatively high number of new pulsators with low fluxes likely reflects the average flux of the *Chandra* point sources (Evans et al. 2010; Wang et al. 2016). At any rate, this is a testament of the effectiveness of periodicity search as a tool to infer the nature of faint objects.

The third panel of Figure 5, where the periods are plotted against the flux, shows an empty region corresponding to sources with short period and low fluxes. In fact, though we discovered very faint pulsators below 10^{-13}erg cm^{-2} s^{-1} with periods above $\sim$3 000s, we did not detect any pulsator with similar fluxes but shorter periods. This lack is not due (only) to poor statistics given that pulsators with similar number of photons but longer periods were reported in Table 1. Since there is not an obvious bias against these detections, a possible interpretation could be in terms of a magnetic gating mechanism (e.g. Campana et al. 1998; Perna et al. 2006 and references therein). Whether or not a magnetized compact object accretes on its surface depends from the comparison between to distances: the corotation radius $r_{\rm cor}$ and the magnetospheric radius $r_{\rm mag}$. The former marks the distance at which the balance between the centrifugal forces and the local gravity is satisfied and it is defined as:

$$r_{\rm cor} = \left(\frac{GM_X P^2}{4\pi^2}\right)^{1/3} \quad (1)$$

where M_X and P are the mass and spin period, respectively, of the compact object. The latter marks the distance where the balance between the magnetic pressure and the ram pressure of the infalling material and can be written as follows:

$$r_{\rm mag} = \mu^{4/7}(2GM_X)^{-1/7}\dot{M}^{-2/7} \quad (2)$$

where μ is the magnetic moment of the compact object and $\dot{M}$ the rate of infall matter (Ghosh et al. 1977). From the relations above, it is evident that the higher the magnetic field of the compact objects, the larger the infalling mass rate must be to win the centrifugal force of the rotating magnetosphere, to accrete efficiency on the surface of the compact objects and to emit X-rays modulated at the spin period (corresponding to the physical condition that the corotation radius is larger than the magnetospheric one, $r_{\rm cor} < r_{\rm mag}$).

In this scenario, the deficiency of short-period persistent pulsators at low fluxes is not surprising (the only four objects falling in the depleted zone are transient or variable sources). Nonetheless, we also warn the reader that the underabundance of accreting NSs with respect to CVs (with intrinsically longer periods and lower fluxes) might also play an important role in depleting the region corresponding to sources with short period and low fluxes.

In principle, a luminosity–spin period diagram might be an useful tool to estimate $r_{\rm mag}$ and thus to obtain a lower limit on the magnetic field of the compact object. However, in order to draw firm conclusions, other key information are needed. In particular the distances, to convert the fluxes into luminosities, and the orbital or spin nature of the modulations (which is not always straightforward). Also, a larger statistics would be desirable to better circumscribe the empty area.

Such larger statistics is expected to be achieved by means of similar projects which are currently on-going and aimed at exploiting the *Swift* archive (*Swift* Automatic Timing Survey, aka SATS@BAR) and the *XMM–Newton* data (Exploring the X-ray Transient and variable Sky, aka EXTraS[6]). First results from these projects are reported in Esposito et al. (2014, 2015a) and Esposito et al. (2016), respectively.

ACKNOWLEDGMENTS

The scientific results reported in this article are based on data obtained from the *Chandra* Data Archive. This research has made use of software provided by the *Chandra* X-ray Center (CXC) in the application packages CIAO. We thank the anonymous referee for valuable comments. GLI acknowledges the partial support from ASI (ASI/INAF contracts I/088/06/0 and AAE DA-044, DA-006 and DA-017). PE acknowledges funding in the framework of the NWO Vidi award A.2320.0076 (PI: N. Rea) and is grateful to Patrizia Caraveo for the support received in an important phase of this work. LS acknowledges financial support from PRIN-INAF 2014.

REFERENCES

Abbott B. P. et al., 2016, Phys. Rev. Lett., 116, 061102
Abdo A. A., Ackermann M., Ajello M., Anderson B., Atwood W. B., Axelsson M., Fermi LAT Collaboration, 2009, Science, 325, 840
Atwood W. B., Ziegler M., Johnson R. P., Baughman B. M., 2006, ApJ, 652, L49
Bartlett E., Coe M., Israel G., Clark J., Esposito P., D'Elia V., Udalski A., 2016, submitted to MNRAS
Blackburn J. K., 1995, in ASP Conf. Ser., San Francisco CA, Vol. 77, Shaw, R. A. and Payne, H. E. and Hayes, J. J. E., eds., Astronomical Data Analysis Software and Systems IV., p. 367
Buccheri R. et al., 1983, A&A, 128, 245
Campana S., Colpi M., Mereghetti S., Stella L., Tavani M., 1998, A&A Rev., 8, 279
Corbet R. H. D., Hannikainen D. C., Remillard R., 2004a, The Astronomer's Telegram, 269
Corbet R. H. D., Markwardt C. B., Coe M. J., Edge W. R. T., Laycock S., Marshall F. E., 2004b, Astron. Tel., 273
Currie T., Evans N. R., Spitzbart B. D., Irwin J., Wolk S. J., Hernandez J., Kenyon S. J., Pasachoff J. M., 2009, AJ, 137, 3210
Dall'Osso S., Israel G. L., Stella L., 2006, A&A, 447, 785
Davidge T. J., 1995, AJ, 110, 1177
Edmonds P. D., Gilliland R. L., Heinke C. O., Grindlay J. E., 2003a, ApJ, 596, 1177
Edmonds P. D., Gilliland R. L., Heinke C. O., Grindlay J. E., 2003b, ApJ, 596, 1197
Esposito P. et al., 2016, MNRAS, 457, L5
Esposito P. et al., 2015a, MNRAS, 450, 1705
Esposito P., Israel G. L., Milisavljevic D., Mapelli M., Zampieri L., Sidoli L., Fabbiano G., Rodríguez Castillo G. A., 2015b, MNRAS, 452, 1112
Esposito P., Israel G. L., Sidoli L., Mapelli M., Zampieri L., Motta S. E., 2013a, MNRAS, 436, 3380
Esposito P., Israel G. L., Sidoli L., Mason E., Rodríguez Castillo G. A., Halpern J. P., Moretti A., Götz D., 2013b, MNRAS, 433, 2028
Esposito P., Israel G. L., Sidoli L., Rodríguez Castillo G. A., Masetti N., D'Avanzo P., Campana S., 2013c, MNRAS, 433, 3464

[6] See the project web site at www.extras-p7.eu.

Esposito P., Israel G. L., Sidoli L., Tiengo A., Campana S., Moretti A., 2014, MNRAS, 441, 1126
Evans I. N. et al., 2010, ApJS, 189, 37
Farrell S. A., Murphy T., Lo K. K., 2015, ApJ, 813, 28
Fruscione A. et al., 2006, in SPIE Conference Series, Vol. 6270, Observatory Operations: Strategies, Processes, and Systems, Silva D. R., Doxsey R. E., eds., SPIE, Bellingham, p. 62701V
Galache J. L., Corbet R. H. D., Coe M. J., Laycock S., Schurch M. P. E., Markwardt C., Marshall F. E., Lochner J., 2008, ApJS, 177, 189
Garmire G. P., Bautz M. W., Ford P. G., Nousek J. A., Ricker, Jr. G. R., 2003, in Proceedings of the SPIE., Vol. 4851, X-Ray and Gamma-Ray Telescopes and Instruments for Astronomy., Truemper J. E., Tananbaum H. D., eds., SPIE, Bellingham, pp. 28–44
Ghosh P., Pethick C. J., Lamb F. K., 1977, ApJ, 217, 578
Graham M. J., Drake A. J., Djorgovski S. G., Mahabal A. A., Donalek C., Duan V., Maker A., 2013, MNRAS, 434, 3423
Grindlay J. E., Heinke C., Edmonds P. D., Murray S. S., 2001, Science, 292, 2290
Haberl F., Eger P., Pietsch W., 2008a, A&A, 489, 327
Haberl F., Eger P., Pietsch W., Corbet R. H. D., Sasaki M., 2008b, A&A, 485, 177
Hannikainen D. C., Rodriguez J., Pottschmidt K., 2003, IAU Circ., 8088
Harris W. E., 1996, AJ, 112, 1487
Heinke C. O., Grindlay J. E., Edmonds P. D., 2005a, ApJ, 622, 556
Heinke C. O., Grindlay J. E., Edmonds P. D., Cohn H. N., Lugger P. M., Camilo F., Bogdanov S., Freire P. C., 2005b, ApJ, 625, 796
Hong J., van den Berg M., Grindlay J. E., Servillat M., Zhao P., 2012, ApJ, 746, 165
in't Zand J., Heise J., Ubertini P., Bazzano A., Markwardt C., 2004, in ESA Special Publication, Vol. 552, 5th INTEGRAL Workshop on the INTEGRAL Universe, Schoenfelder V., Lichti G., Winkler C., eds., p. 427
Israel G. L. et al., 2002, A&A, 386, L13
Israel G. L., Mereghetti S., Stella L., 1994, ApJ, 433, L25
Israel G. L., Stella L., 1996, ApJ, 468, 369
Israel G. L., Stella L., Angelini L., White N. E., Kallman T. R., Giommi P., Treves A., 1997, ApJ, 474, L53
Israel G. L., Treves A., Stella L., Angelini L., White N. E., Kallman T., Covino S., Giommi P., 1998, in NATO Advanced Science Institutes (ASI) Series C, Buccheri R., van Paradijs J., Alpar A., eds., Vol. 515, Dordrecht - Boston, Kluwer Academic Publishers, p. 411
Knigge C., Baraffe I., Patterson J., 2011, ApJS, 194, 28
Koenig X., Grindlay J. E., van den Berg M., Laycock S., Zhao P., Hong J., Schlegel E. M., 2008, ApJ, 685, 463
Lamb R. C., Macomb D. J., Prince T. A., Majid W. A., 2002, ApJ, 567, L129
Lanzoni B. et al., 2010, ApJ, 717, 653
Laycock S., Zezas A., Hong J., Drake J. J., Antoniou V., 2010, ApJ, 716, 1217
Leahy D. A., Darbro W., Elsner R. F., Weisskopf M. C., Kahn S., Sutherland P. G., Grindlay J. E., 1983, ApJ, 266, 160
Lin D., Webb N. A., Barret D., 2014, ApJ, 780, 39
Mereghetti S., Pintore F., Esposito P., La Palombara N., Tiengo A., Israel G. L., Stella L., 2016, MNRAS, 458, 3523
Mereghetti S., Tiengo A., Esposito P., La Palombara N., Israel G. L., Stella L., 2009, Science, 325, 1222
Muno M. P., Baganoff F. K., Bautz M. W., Brandt W. N., Garmire G. P., Ricker G. R., 2003, ApJ, 599, 465
Muno M. P., Gaensler B. M., Nechita A., Miller J. M., Slane P. O., 2008, ApJ, 680, 639
Nichelli E. et al., 2011, in Swift and the Surprising Sky: The First Seven Years of Swift. Online at: http://www.brera.inaf.it/docM/OAB/Research/SWIFT/Swift7/Presentations/Nichelli.pdf, p. 39
Perna R., Bozzo E., Stella L., 2006, ApJ, 639, 363
Rosen S. R. et al., 2016, A&A, 590, A1
Scargle J. D., 1982, ApJ, 263, 835
Sidoli L., Esposito P., Motta S. E., Israel G. L., Rodrigúez Castillo, 2016, MNRAS, 460, 3637
Torrejón J. M., Negueruela I., Smith D. M., Harrison T. E., 2010, A&A, 510, A61
Turolla R., Zane S., Watts A. L., 2015, Reports on Progress in Physics, 78, 116901
van den Berg M., Penner K., Hong J., Grindlay J. E., Zhao P., Laycock S., Servillat M., 2012, ApJ, 748, 31
Wang S., Liu J., Qiu Y., Bai Y., Yang H., Guo J., Zhang P., 2016, ApJS, 224, 40
Watson M. G. et al., 2009, A&A, 493, 339
Wen L., Levine A. M., Corbet R. H. D., Bradt H. V., 2006, ApJS, 163, 372

This paper has been typeset from a TEX/ LATEX file prepared by the author.

Table A1. Datasets used for the timing analysis reported in this work.

Name	Observation ID	
	Chandra	*XMM–Newton*
CXO J002415.9–720436	78 ,953 ,955 ,956 ,2735 ,2736 ,2737 ,2738 ,3384 ,3385 ,3386, 15747 ,15748 ,16527 ,16529 ,17420	…
CXOU J004814.1–731003	2945 ,14674	0110000101, 0403970301, 0404680101
CXOU J005048.0–731817	2945 ,3907 ,7156 ,8479 ,11095 ,11096 ,11097 ,11980 ,11981, 11982 ,11983 ,11984 ,11985 ,12200 ,12208 ,12210 ,12211, 12212 ,12215 ,12216 ,12217	…
CXOU J005440.5–374320	16028 ,16029	…
CXOU J005758.4–722229	13773 ,14671 ,15504	0700580401
CXO J021950.4+570518	5407 ,5408 ,9912 ,12021	0201160201
CXOU J055930.5–523833	12264 ,13116 ,13117	0604010301
CXOU J063805.3–801854	14925	…
CXOU J091539.0–495312	14544 ,16603	…
CXOU J111133.7–603723	2782 ,12972 ,14822 ,14823 ,14824 ,16496 ,16497	0051550101
CXOU J112347.4–591834	126 ,6677 ,6678 ,6679 ,6680 ,8221 ,8447	0110012701, 0400330101, 0743980101
CXO J123030.3+413853	1579 ,1579 ,4725 ,4725 ,4726	0112280201, 0556300101
CXOU J123823.4–682207	11308	…
CXOU J141332.9–651756	12823 ,12824	0111240101
CXO J141430.1–651621	355 ,356 ,12823 ,12824	0111240101
CXOU J153539.8–503501	9956	…
CXO J161437.8–222723	7509	0404790101
CXOU J163855.1–470145	12516 ,12517	0303100101
CXO J170113.3+640757	547 ,8032 ,8033 ,9756 ,9757 ,9758 ,9759 ,9760 ,9767	0107860301
CXO J170214.7–295933	3795 ,5469 ,6337 ,8984 ,13711 ,14453	…
CXO J170227.3–484507	4445 ,4446	0111360501, 0112900201
CXO J171004.6–321205	4549, 16708	…
CXOU J173037.7–212633	4650 ,6714 ,6715 ,6716 ,6717 ,6718 ,7366 ,16004 ,16614	…
CXOU J173113.7–212552	6714 ,6716	0084100101
CXO J173359.0–220614	4583	…
CXOU J174042.3–534029	79, 2668, 2669, 7460, 7461	…
CXO J174245.1–293455	2283 ,7043	…
CXO J174638.0–285325	945, 7048, 14897, 17236	0202670801, 0658600101
CXOU J174811.0–244930	14625 ,15615	…
CXOU J180839.8–274131	15794	…
CXO J180900.0–435039	3779	…
CXOU J181516.4–270851	16505 ,16506	…
CXOU J181924.1–170607	12348	0402470101 0604820101, 0693900101
CXO J184441.7–030549	8163 ,11232 ,11801	0046540201, 0602350101, 0602350201
CXOU J185415.8–085641	14585	…
CXOU J191043.7+091629	13440 ,13441	0084100401, 0084100501
CXO J193437.8+302524	587	0723570401
CXOU J204734.8+300105	740	0082540701
CXOU J215447.8+623155	8938 ,10818 ,10819 ,10820	…
CXOU J215544.5+380116	3967 ,12879 ,13218	…
CXOU J225355.1+624336	9919 ,9920 ,10810 ,10811 ,10812	0743980301
CXO J165334.4–414423	6291	0109490101, 0109490201, 0109490301, 0109490401, 0109490501, 0109490601
CXO J174728.1–321443	4566 ,4567 ,13580	0743980401
CXO J182531.4–144036	4600 ,5341	0505530101
CXO J191404.2+095258	4590	0761690301

APPENDIX A: ARCHIVAL DATA

For sake of completeness we list, for each source in Table A1, the corresponding observation(s) we used for the timing analysis and to infer the fluxes.